# A Photoelectric Detector Suspended under a Balloon for Actinic Flux Measurements

J. C. H. VAN DER HAGE, W. BOOT, H. VAN DOP, P. G. DUYNKERKE, AND J. VILÀ-GUERAU DE ARELLANO

*Institute for Marine and Atmospheric Research, Utrecht University, Utrecht, the Netherlands*

(Manuscript received 1 March 1993, in final form 7 September 1993)

ABSTRACT

An instrument to measure ultraviolet actinic flux in and outside clouds was constructed and calibrated. Characteristics of the instrument are: 1) it is equipped with gallium phosphide photodiodes, 2) its isotropic directional response is almost perfect due to the special design of the optical diffusers, and 3) it is a lightweight construction (150 g) allowing the use of a balloon or a kite as an observation platform.

Ground-level observations and vertical profiles, measured with this UV photometer in clear air and in stratocumulus during the Atlantic Stratocumulus Transition Experiment in the Azores, confirm that the Madronich radiation transfer model is valid for clouds.

## 1. Introduction

The photodissociation of $NO_2$ is the only process by which ozone is formed in the troposphere including the atmospheric boundary layer (Leighton 1961; Warneck 1988). It is responsible for roughly 50% of the total tropospheric ozone and is the dominant mechanism for the formation of photochemical smog. Photodissociation of $NO_2$ yields $O_3$ after the atom O produced by photolysis reacts with $O_2$ (Finlayson-Pitts and Pitts 1986). The photodissociation rate of $NO_2$ is proportional to the actinic flux in the spectral region that ranges from 320 to 420 nm, the UV-A range. The rate of photolysis of $NO_2$ can be calculated experimentally with a chemical actinometer, a tube containing photochemically reactive compounds that are exposed to radiation (Stedman and Jackson 1975). An alternative way of calculating the photolysis rate is to measure the actinic flux, which is the solar radiation integrated over all solid angles in a given spectral range. In clear cloudless conditions actinic flux can be derived from global radiation, the irradiance on a horizontal surface (Bahe et al. 1980; Madronich 1987). However, in (partly) cloudy or (moderately) polluted conditions it is advisable to measure the actinic flux directly.

Nader and White (1969) and later Guicherit (1978) designed photoelectric detectors consisting of six light sensors in a cubic array. They showed that ultraviolet actinic flux on the ground is strongly influenced by atmospheric conditions. More recently Junkermann et al. (1987) constructed a photoelectric detector suitable for mounting on airplanes. On regional and global scales the surface albedo and cloud cover strongly influence the actinic flux. Mathematical models of photochemical and transport processes on these scales should therefore include an accurate description of the actinic flux intensities as a function of location and height.

Vertical profiles of the ultraviolet actinic flux in and above clouds can be measured from aircraft (Dickerson et al. 1982), but the climbing capacities of aircraft are limited and consequently one vertical profile requires several horizontal traverses, which disturbs the cloud in the process to an unknown extent. On the other hand, a tethered balloon or even a kite can be moved up and down through a cloud without leaving turbulent wakes of heat and vapor.

The present paper describes a new photoelectric actinic flux meter for measuring fluxes in the UV-A region. The instrument is designed to be used under a tethered balloon but can also be used to take surface measurements.

## 2. Description of the instrument

The ultraviolet actinic flux sensor is housed in a plastic cylinder 60 mm × 53 mm with thin walls, from which six tubes protrude, each being 32 mm long and 11 mm wide. These tubes represent six identical optical receivers perpendicular to each other. Each receiver contains a gallium phosphide diode (Hamamatsu®, GaP1962) covered by a UV-transmitting black glass window (Schott®, UG 1) and a Teflon diffuser (*a*, *b* and *c* in Fig. 1). The photocurrents of the diodes are fed to six current–voltage converters incorporated in two operational amplifiers (TL 1078) with low temperature drift and low power consumption. Summation of the output voltages results in one final signal that is transmitted to the ground through one of the channels

*Corresponding author address:* Dr. J. C. van der Hage, Institute of Marine and Atmospheric Research, Utrecht University, Post Bus 80.005, 3508 TA Utrecht, the Netherlands.

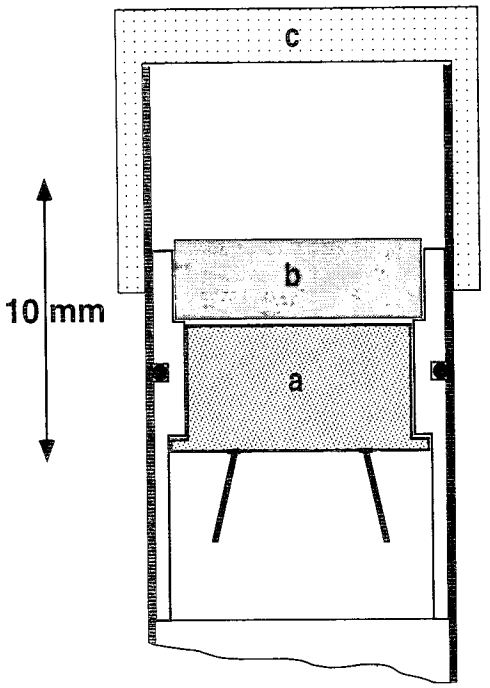


FIG. 1. Cross section of an individual receiver of the UV photometer: *a*—GaP 1962 photodiode; *b*—UG1 glass filter, black for visible light but transparent between 300 and 400 nm; *c*—Teflon diffuser. The location of the combination *a* and *b* is variable with respect to *c* so that the sensitivity of the receiver can be adjusted.

of a radiosonde attached to the balloon. To economize on weight, the electronics are powered from the battery in the radiosonde. The total weight of the actinic flux sensor including the suspension cable is slightly less than 150 g.

The 10-m suspension cable guarantees that the balloon with dimensions of 3 m × 1 m can obscure only a solid angle smaller than 1% of the upward field of view. In diffuse radiation, the actinic flux can therefore be measured with only negligible error due to the shadow of the balloon. In clear-sky situations, there is a small probability that the sun will disappear behind the balloon and falsify the measurements, but when this occurs the error is so great that it can easily be recognized and removed from the record.

## 3. Directional response of the UV photometer

An ideal photometer to measure actinic flux is isotropic with regard to the direction of incident radiation. The sensor we developed is arranged according to cubic symmetry (sixfold). If all six receivers were identical and with a perfect cosine response, then the total response of the instrument to light coming from one direction would be proportional to the surface area of a cube projected on a plane perpendicular to that particular direction. In other words, the sensitivity would be at its maximum in the directions of the body diagonals and at its minimum in the directions perpendicular to the cube faces. Cubic geometry therefore prescribes a ratio of $\sqrt{3}:1 \cong 1.73$ for the maximum and minimum sensitivity. A maximum is found in eight positions, corresponding to the corners of the cube, and minima are found in only six positions. The angle between a maximum and a nearest-minimum position is about 55°.

The directional response of the sixfold sensor as a whole can be improved in the isotropic sense by installing receivers with a specific angular response that deviates from a perfect cosine response. These improved receivers should underestimate radiance incident at $\theta \cong 55°$ and they should overestimate radiance entering at $\theta \cong 90°$. Diffusers with various geometries were tried out on an optical bench and although the ideal diffuser was not found, circular Teflon caps with dimensions as indicated in Fig. 1 resulted in the ratio of maximum to minimum sensitivity being below 1.1 instead of 1.73 for the sixfold sensor as a whole. Figure 2 shows the directional response measured for such an improved individual diffuser.

The directional response of the complete photometer can be calculated from the angular responses measured for the six individual receivers, shown in Fig. 2. The individual response functions are identical; therefore, the response function of any single receiver can be denoted by $f(\gamma)$, in which $\gamma$ is the angle between the incident radiation $I$ and the direction in which the receiver is pointing. The response function $r(\varphi, \theta)$ of the whole instrument, consisting of six receivers, can be written in the following manner:

$$r(\varphi, \theta) = f(\theta) + f(\alpha) + f(\beta) + f(\pi - \theta) + f(\pi - \alpha) + f(\pi - \beta), \quad (1)$$

where the angles $\varphi$, $\theta$, $\alpha$, and $\beta$ are explained in Fig. 3.

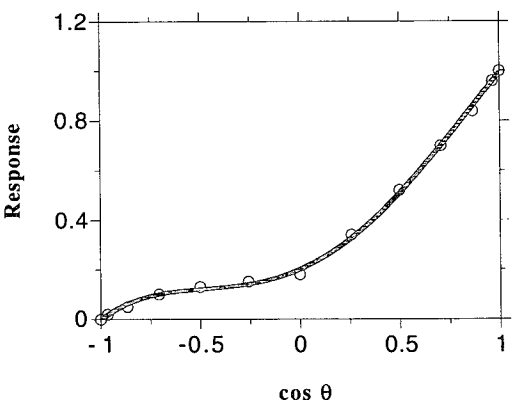


FIG. 2. Relative directional response measured for the UV receivers with Teflon diffusers as shown in Fig. 1. The continuous line is a fourth-order polynomial curve fit to the data. Here $\theta$ is the angle between the receiver axis and the incident radiation; note that the improved receiver is sensitive to light coming from angles larger than 90°.

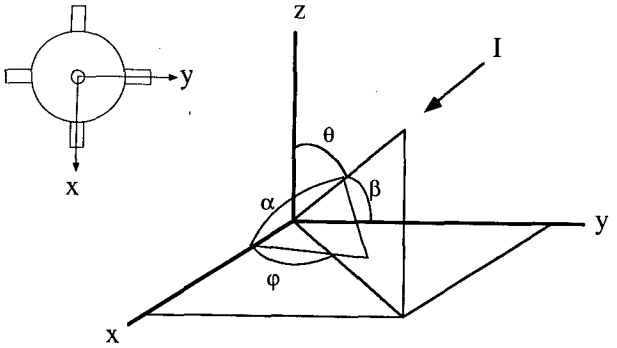


FIG. 3. Relevant angles between the incident radiation $I$ and the receivers of the photometer. The insert on the left-hand side of the figure represents a top view of the photometer. The instrument body is a cylinder; the receivers protrude in the $x$, $y$, and $z$ directions.

For the theoretical case where a single receiver has a perfect cosine response $f(\gamma) = \cos(\gamma)$, the response function, Eq. (1), can be written as

$$r(\varphi, \theta) = \cos\theta + \sin\theta(\cos\varphi + \sin\varphi). \quad (2)$$

In the case of the perfect cosine response, only three receivers are taken into account; that is, a negligible signal is measured by the receiver for angles larger than 90°. The response function Eq. (2) has a maximum value of $r = \sqrt{3}$ at $\varphi = 45°$ and $\theta \approx 55°$.

However, the actual receivers of the photoelectric detector have a directional response as shown in Fig. 2. This curve has been fitted by a fourth-order polynomial, which was then substituted in Eq. (1). Because the response of a single sensor is now larger than zero at $\theta \geq 90°$, all six sensors have to be taken into account to calculate the angular response of the whole instrument. Figure 4 shows the calculated angular response of the complete photometer as a function of the angles $\varphi$ and $\theta$. This response function has an average value of $1.9 \pm 0.1$, so deviations from isotropy are about 5%.

In this calculation the shading effects and reflections caused by the photometer body are neglected. Nevertheless, the calculated response function corresponds quite well to the angular response measured in the field in the Azores (see section 5).

## 4. Spectral response

The spectral response of the receivers is determined by the gallium phosphide photodiode GaP 1962, together with the black UG1 glass filter and the Teflon cap. In Fig. 5, $a$ is the response curve of the diode as indicated by the manufacturer; $b$ represents the spectral transmission of a UG1 filter 3.5 mm thick, calculated from data given by Schott (1982) for a 1-mm UG1 filter, and $c$ is the spectral transmission of 2-mm-thick Teflon, calculated from data given by Saunders and Kostkowsky (1989). The curves in Fig. 5 are drawn on different arbitrary scales because $a$ does not have

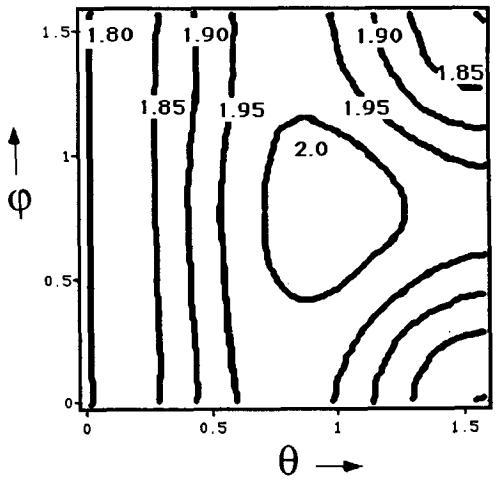


FIG. 4. Calculated angular response of the photometer with the improved receivers.

the same dimension as $b$ or $c$. The heavy curve $r$ (V $W^{-1}$ $m^2$ nm) is the product of $a$, $b$, and $c$ and represents the spectral response of a receiver as a whole. The response curve $r$ has a maximum at 360 nm with a bandwidth of ±25 nm, and 90% of the total surface under curve $r$ is found between 330 and 390 nm.

## 5. Calibrating the photometer

Before calibration all six receivers must be adjusted until they have equal sensitivities. The sensitivity of a receiver depends on the location of the diode relative to the Teflon diffuser. A diode and a UG1 filter ($a$ and $b$, respectively, in Fig. 1) are mounted together in a

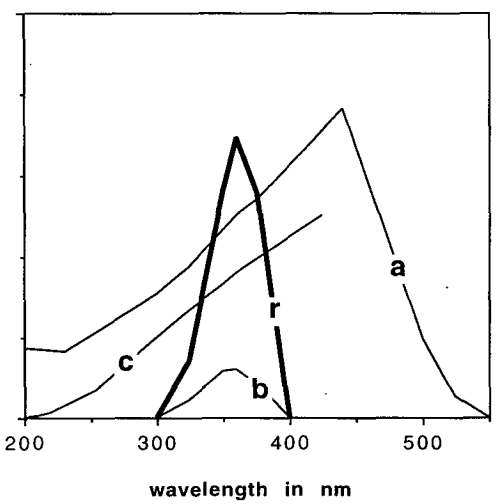


FIG. 5. Spectral response of a UV receiver: $a$ (A $W^{-1}$)—spectral response of the Hamamatsu GaP 1962 photodiode; $b$ (%)—transmission of a 3.5-mm UG1 glass filter; $c$ (%)—transmission of 2-mm-thick Teflon sheet; $r$ (V $W^{-1}$ $m^2$ nm)–resulting spectral response.

small cylinder that can be pushed up or down through the tube. This does not affect the angular characteristics of the receiver as long as the distance between the diffuser and the UG1 filter ($b$ and $c$ in Fig. 1) remains larger than 1.2 mm. When one receiver is exposed to a constant illumination, while the other five are shielded from the light, the output signal of the photometer can be adjusted to a predefined value by moving the cylinder in the tube. This procedure was repeated for each receiver to get an optimum isotropic response. The photoelectric detector was then calibrated against a UV-irradiance instrument that operates continuously at the Royal Dutch Meteorological Institute (KNMI). That instrument is a prototype of the Kipp® CUA-1 ultraviolet radiometer, which is expected to become commercially available in 1993. It measures total and direct downward irradiance at 367 nm with a bandwidth of ±5 nm. Madronich (1987) pointed out the physical differences and relationships between the radiative quantities, irradiance, and actinic flux. When there is no direct radiation the relation between downward irradiance $E_d$ and actinic flux $F_d$ is given by

$$F_d = (2\alpha + 2)E_d. \tag{3}$$

At the KNMI site, the albedo $\alpha$ for UV-A radiation was very small, it was 0.05. Consequently, for diffuse radiation only,

$$F_d = 2.1E_d. \tag{4}$$

Taking advantage of this linear relationship, the calibration was carried out during two overcast days, in such conditions more than 98% of the total radiation was diffuse.

The angular response of the photometer was also tested in the field (in the Azores). Under clear sky conditions, the instrument was rotated over different angles. A variation of less than 5% was found for any angle; that is, the response of the photometer is practically independent of the angle of incidence. Therefore, the calibration made for purely diffuse light is also applicable to conditions involving direct radiation.

## 6. Measurements

The photometer was used during the Atlantic Stratocumulus Transition Experiment (ASTEX 1992) field campaign conducted in the Azores in June 1992. The measurements were taken on a surface site on Santa Maria Island (36.99°N, 25.17°W, 50 m MSL) close to the airport. The objective of ASTEX was to study the marine and stratocumulus clouds in this region, their physical and radiative properties, and their effects on the atmosphere and ocean. Within this experimental framework, two studies were performed with the photometer: these involved diurnal variation measurements at ground level and tethered-balloon soundings.

### *a. Diurnal variations*

The diurnal variation of the actinic flux is typically different from the diurnal variation of the global radiation. To obtain a time series for the actinic flux from sunrise to sunset, we attached the photometer to a mast 1.5-m above ground level. Simultaneously, global radiation measurements were made at the same height with a Kipp® CM14 pyranometer. This pyranometer measures the irradiance for wavelengths between 305 and 2800 nm with a precision of 2 W $m^{-2}$. Figure 6 shows the observations for both quantities measured on 19 June under a cloud-free sky. The global radiation measurements were averaged every 30 min. Because the photometer was also used with the tethered balloon and because the balloon measurements had first priority, measurements were taken on three different days (19, 26, and 27 June) in order to obtain a complete actinic flux time series. The data presented were averaged every minute. The presence of isolated clouds explains the scatter of the measurements around 1500 and 1800 UTC. Figure 6 shows the different behavior of the two radiative quantities. When there is only direct radiation, the actinic flux $F_0$ should vary in time like a step function, maintaining a constant value from sunrise to sunset due to the independence of this quantity from the solar zenith angle $\theta_0$. The relation between the direct irradiance and the actinic flux is then

$$F_0 = \frac{E_0}{\cos\theta_0} \tag{5}$$

and $E_0 \approx S\cos\theta_0$, where $S$ is the irradiance at the top of the atmosphere ($S$ is usually called the solar constant).

This step function characteristic can be recognized faintly in the actinic flux measurements in Fig. 6. Between 1200 and 1530 UTC, the actinic flux is almost constant, varying by less than 5%. Similar results were

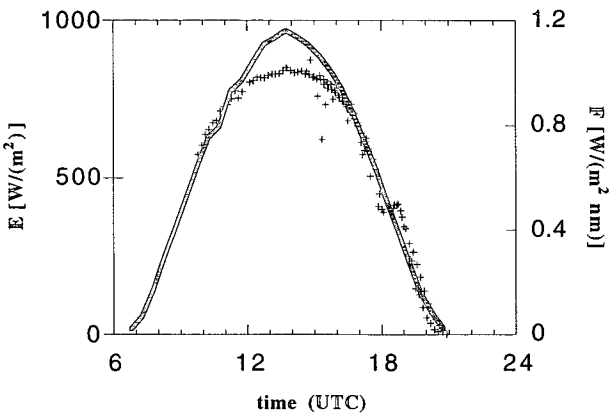


FIG. 6. Diurnal variation of global radiation $E$ (continuous line), and actinic flux $F$ (cross symbols) at ground level under clear sky conditions.

found by Nader and White (1969) in a comparative study of UV horizontal and volumetric measurements. In addition, the actinic flux in Fig. 6 decays more sharply than the global radiation measurements. The difference between Fig. 6 and a step function is due mainly to the contribution of diffuse radiation. The complete relation between the actinic flux and the components of the irradiance (direct and diffuse) is given by Madronich:

$$F = \left(2\alpha + \frac{1}{\cos\theta_0}\right)E_0 + (2\alpha + 2)E_d. \qquad (6)$$

Note that expressions (4) and (5) are limiting cases of expression (6), particularly so when reflected light is ignored. At the Santa Maria site the UV albedo was indeed very small; $\alpha \approx 0.05$. The contribution of the diffuse irradiance is dependent on the zenith angle of the sun. For the Azores during the month of June, one can estimate that 65% of the total radiation is direct, but UV radiation is scattered more strongly than the other wavelengths. Consequently significantly less than 65% of the UV radiation was direct during the time series measurements. To obtain a completely constant value for the actinic flux during a whole day, all the radiation (100%) has to be direct.

### b. *Tethered-balloon soundings*

To determine the actinic flux vertical profile in clear sky conditions and in the presence of clouds, we attached the photometer 10 m below a tethered balloon. At that distance, the actinic flux measurements are hardly influenced by the presence of the balloon. Only when the sun disappears behind the balloon all direct radiation is blocked. However, in such cases, abnormal values are obtained and these are identified and rejected without difficulty. Using radiative transfer models, Madronich (1987) and Van Weele and Duynkerke (1993) have demonstrated that actinic flux varies with cloud conditions. With a clear sky as a reference, the model results suggest lower values for the actinic flux below the cloud, a linear increase in the cloud and higher values above the cloud.

Figure 7 shows two soundings: one under clear sky, and the other under cloudy conditions. The clear-sky and overcast soundings started at 1737 UTC ($\theta_0 = 52°$) and at 1603 UTC ($\theta_0 = 34°$), respectively. For the last sounding, mostly broken to overcast (7/8 and 8/8), marine stratocumulus was present during the measurements. There were no higher clouds above the stratocumulus. Details of cloud properties were provided by The Pennsylvania State University (Albrecht, personal communication in the ASTEX environment). The cloud-base height was 575 m and the cloud-top height was 850 m. In addition, the integrated liquid water path was $1.4 \times 10^{-4} \pm 3 \times 10^{-5}$ m. An average value of 10 $\mu$m was measured for the effective radius; this

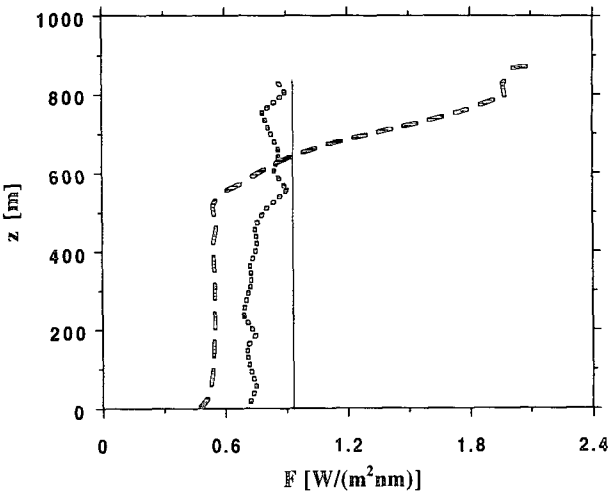


FIG. 7. Measured vertical profiles of actinic flux $F$ for clear sky (dotted line) and cloudy sky (dashed line) and the theoretical vertical profile of actinic flux calculated using Eq. (6) (continuous line).

value is based on in-cloud aircraft observations taken during ASTEX (Johnson et al. 1993). As the figure shows, the observations reflect the different characteristics of the actinic flux under clear sky and cloud conditions. For the former, the actinic flux slightly increases throughout the complete sounding. For the latter, a lower value compared to the clear-sky case is found below the cloud. An approximately linear increase is observed as the instrument moves up through the cloud. The theoretical maximum of actinic flux below cloud top (Madronich 1987) is difficult to detect due to cloud inhomogeneities. At cloud top, and compared with clear-sky measurements at the surface and at the same solar zenith angle, a 2.41 enhancement factor of the actinic flux was observed. Although, a proper comparison must be done with the actinic flux measured at the same height, the uncertainty introduced by the use of the clear-sky value measured at the surface is less than 10%.

Finally, using expression (6), one can calculate the clear-sky value of the actinic flux at the same solar zenith angle and ground albedo (the continuous line in Fig. 7). The value found is 0.91 W m$^{-2}$ nm$^{-1}$. Therefore, the presence of a cloud with an optical depth of 23 decreases the actinic flux below the cloud by a factor 0.62 and enhances the actinic flux at cloud top by a factor 2.3.

These observations correspond within 15% to the theoretical profiles calculated with the models referred to above. This is the first time that these models have been verified in situ. The observations show that the instrument is able to produce accurate measurements in and outside clouds. A complete description and analysis of the measurements during the ASTEX experimental field campaign will be published elsewhere (Vilà-Guerau de Arellano and Duynkerke 1994).

*Acknowledgments.* The authors wish to thank the Netherlands Organization for Scientific Research (NWO), the National Programme on Global Biosphere (NOP), and Dr. Wayne Schubert (Colorado State University) for supporting their participation in the ASTEX experiment. Penn State University provided the necessary cloud data: special thanks to Bruce Albrecht, Dennis Thomson, and Mark Miller. One of the authors, Han van Dop, is supported by the Ministry of Education and Science.

## REFERENCES

ASTEX Operations Plan, 1992: Available from the FIRE Project Office, MS 483, NASA Langley Research Center, Hampton, VA 23665-5225.

Bahe, F. C., U. Schurat, and K. H. Becker, 1980: The frequency of $NO_2$ photolysis at ground level as recorded by a continuous actinometer. *Atmos. Environ.*, **14,** 711–718.

Dickerson, R. R., D. H. Stedman, and A. C. Delany, 1982: Direct measurements of ozone and nitrogen dioxide photolysis rates in the atmosphere. *J. Geophys. Res.*, **87,** 4933–4946.

Finlayson-Pitts, B. J., and J. N. Pitts, 1986: *Atmospheric Chemistry: Fundamental and Experimental Techniques.* John Wiley & Sons, 1096 pp.

Guicherit, R., 1978: Photochemical smog formation in the Netherlands. TNO Publication, Delft, the Netherlands. [Available from Postbus 6011, 2600 JA, Delft, the Netherlands.]

Johnson, D. W., G. M. Martin, J. Taylor, and M. Gibbs, 1993: ASTEX flight summary for U.K. C-130. Meteorological Research Flight. British Meteorological Office.

Junkermann, W., U. Platt, and A. Volz-Thomas, 1987: A photoelectric detector for the measurement of photolysis frequencies of ozone and other atmospheric molecules. *J. Atmos. Chem.*, **8,** 203–227.

Leighton, P. A., 1961: *Photochemistry of Air Pollution.* Academic Press, 300 pp.

Madronich, S., 1987: Photodissociation in the atmosphere. 1: Actinic flux and the effects of ground reflections and clouds. *J. Geophys. Res.*, **92,** 9740–9752.

Nader, J. S., and N. White, 1969: Volumetric measurement of ultraviolet energy in an urban atmosphere. *Environ. Sci. Tecnol.*, **3,** 848–854.

Saunders, R. D., and H. J. Kostkowski, 1989: Roughened quartz surfaces and Teflon as small angle diffusers and depolarizers between 200 and 400 nm. *Appl. Opt.*, **28,** 3242–3245.

Schott, 1982: Farb- und Filterglas für Wissenschaft und Technik. Schott Glaswerke Nr. 3531/4d, Schott, Mainz, Germany. [Available from Postfach 2480 D 6500, Mainz, Germany.]

Stedman, D. H., and J. O. Jackson, 1975: The photostationary state in photochemical smog. *Int. J. Chem. Kinetic Symp.*, **1,** 493–501.

Van Weele, M., and P. G. Duynkerke, 1993: Effect of clouds on the photodissociation of $NO_2$: Observations and modelling. *J. Atmos. Chem.*, **16,** 231–253.

Vilà-Guerau de Arellano, J., and P. G. Duynkerke, 1994: Tethered-balloon measurements of actinic flux in a cloud-capped marine boundary layer. *J. Geophys. Res.*, in press.

Warneck, P., 1988: *Chemistry of the Natural Atmosphere.* Vol. 41, *International Geophysics Series.* Academic Press, 757 pp.